City Research Online

City St George's, University of London

Citation: Le, B. T., Nguyen, T. T. T., Divall, S. & Davies, M. C. R. (2023). A study on large volume losses induced by EBPM tunnelling in sandy soils. Tunnelling and Underground Space Technology, 132, 104847. doi: 10.1016/j.tust.2022.104847

This is the accepted version of the paper.

This version of the publication may differ from the final published version. To cite this item please consult the publisher's version.

Permanent repository link: https://openaccess.city.ac.uk/id/eprint/29167/

Link to published version: https://doi.org/10.1016/j.tust.2022.104847

Copyright and Reuse: Copyright and Moral Rights remain with the author(s) and/or copyright holders. Copies of full items can be used for personal research or study, educational, or not-for-profit purposes without prior permission or charge, unless otherwise indicated, provided that the authors, title and full bibliographic details are credited, a hyperlink and/or URL is given for the original metadata page and the content is not changed in any way. For full details of reuse please refer to City Research Online policy.

City Research Online: http://openaccess.city.ac.uk/ publications@citystgeorges.ac.uk

A study on large volume losses induced by EBPM tunnelling in sandy soils

Authors

B. T. Le, T. T. T. Nguyen, S. Divall, M. C. R. Davies

Abstract

Tunnelling-induced ground surface settlements can be described by a Gaussian distribution curve with two key factors; the displacement trough width and the volume loss. In most cases the volume losses are well-controlled with maximum settlements less than the allowable limits. However, there have been reports showing abnormally large ground surface settlement, in sandy soil, induced by Earth Pressure Balance Tunnel Boring Machines (EPB TBMs). This research reports field data obtained during the construction of the Metro Line 1 Ben Thanh – Suoi Tien Tunnels in Ho Chi Minh city, Vietnam. Data include ground settlement measurements, the geotechnical conditions and TBM operation parameters. The results show that in locations where large settlements had occurred there were common characteristics of high liquefaction index, large excess pore pressure and abnormally large tail void grouting. A novel equation is suggested to describe the relationship between the volume loss and the liquefaction potential index. This has been calculated using simple and commonly available geotechnical parameters for use in practice as an indicator for potentially large settlements caused by EBP TBM tunnelling in sandy soils.

Keywords

EPB TBM; Ground movements; Tunnelling; Case study

LIST OF SYMBOLS AND ABBREVIATION

α	Peak ground acceleration
$\Delta\sigma_F$	Change in face pressure
Δu	Change in pore-water pressure
ε_a	Axial strain
σ_F	Pressure at the TBM face
σ'_h	Horizontal effective stress
σ'_{h0}	Initial horizontal effective stress
σ_v	Vertical total stress
σ'_v	Vertical effective stress
σ'_{v0}	Initial vertical effective stress
γ_d	Reduction coefficient
$C_1 \& C_2$	Coefficients considering the fine contents F_c
C_w	Coefficient defined according to the type of the seismic motion
D	Excavation diameter
D_{50}	Mean grain diameter
D_r	Relative density
EPBM	Earth Pressure Balance Machine
F	Safety rate to liquefaction
FLS	Flow liquefaction surface
FL	Factor of safety to liquefaction
F_c	Fines content
i	Horizontal distance to the point of inflexion
K	Dimensionless settlement trough width parameter
K_0	Earth pressure coefficient at rest
L	Seismic shear stress ratio
N	Raw SPT count at site
N_1	Normalised N-value
N_a	Amended N-value taking into account the effect of grain size
PL	Liquefaction potential index
p'	Mean effective stress
p'_0	Initial mean effective stress
q	Deviatoric stress
R	Dynamic shear strength ratio
R_L	Cyclic triaxial strength ratio
SSL	Steady state line
s	Ground surface settlement
s_{max}	Maximum ground surface settlement
TBM	Tunnel Boring Machine
u	Pore-water pressure
V_{exc}	Volume of the excavation area
V_L	Volume loss
$V_{L(x)}$	Volume loss when the EPBM was at a distance x to the monitoring section
$V - Grout$	Volume of tail void grout per ring
V_S	Volume of the settlement trough
V_t	Volume of ground loss in the region close to the tunnel
$V - Void$	Volume of tail void per ring
$w(z)$	Weight function in accordance with depth z
x	Distance from TBM face to monitoring section (m)
y	Distance from the tunnel centre-line
z	Depth from the ground surface
z_0	Depth from the ground surface to tunnel axis level

INTRODUCTION

Tunnel construction inevitably causes ground movements (**Figure 1**) which, potentially, can result in severe damage to surrounding buildings and buried infrastructure. Therefore, accurate prediction of tunnelling-induced ground deformations is of essential for safe tunnel excavation.

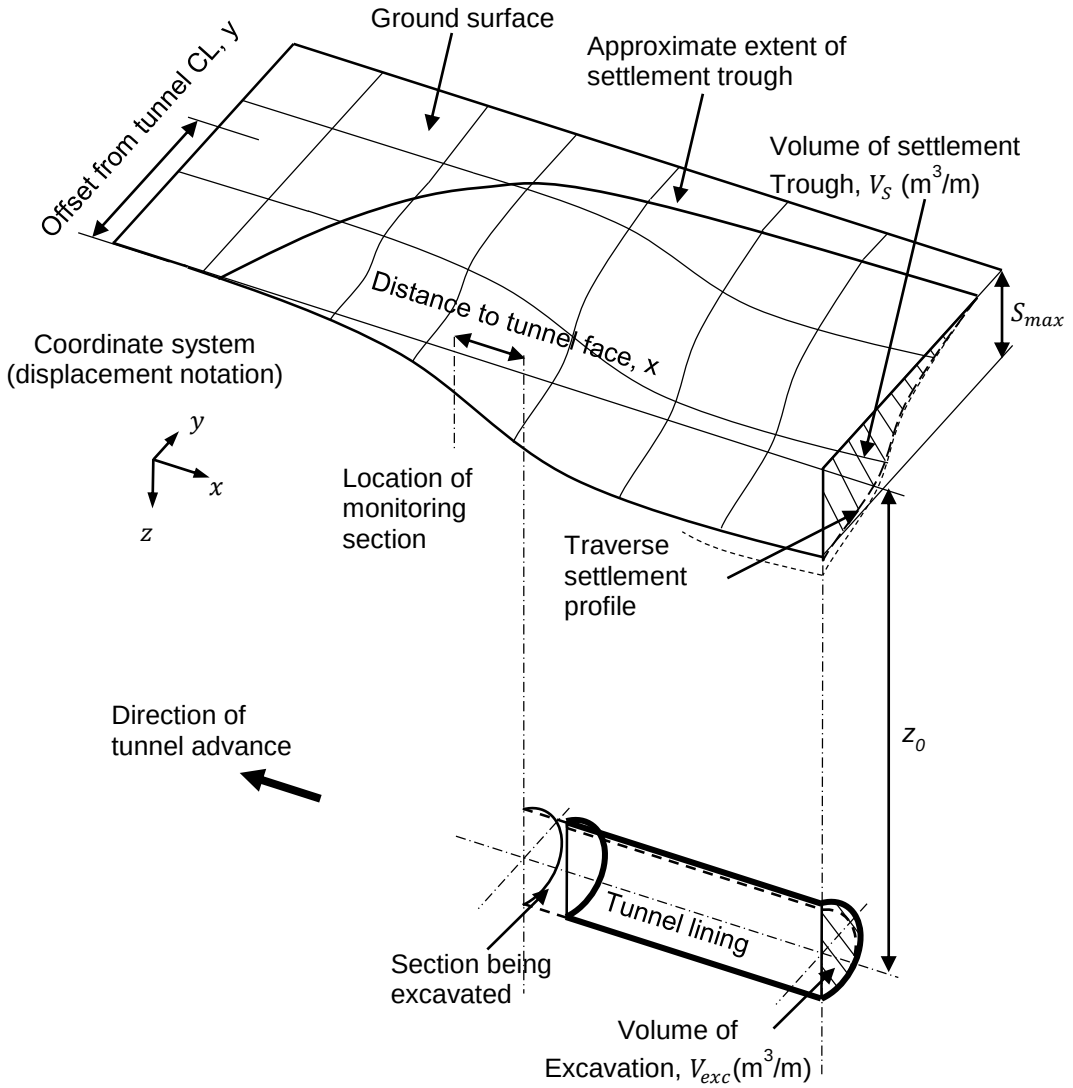

Figure 1. Idealisation of tunnelling induced soil displacement (after Le and Taylor, 2018).

By investigating the field data from case studies, previous research including many studies (Dimmock, 2003; Mair & Taylor, 1997; Nyren, 1998; Peck, 1969; Schmidt, 1969; Shirlaw et al., 2003; Sugiyama et al., 1999; Wan et al., 2017a) have indicated that the ground surface transverse settlement, s, has the shape of a Gaussian distribution curve, as shown in **Figure 2**, and can be described by Equation 1 as below;

$$s = s_{max} exp\left(\frac{-y^2}{2i^2}\right) \quad (1)$$

$$s_{max} = \frac{V_S}{\sqrt{2\pi}i}; \quad (2)$$

where s_{max} is the maximum settlement and normally occurs above the centre-line of the tunnel;

V_S is the volume of the transverse surface settlement trough (**Figure 2**);

y is the distance from the tunnel centre-line;

i is the horizontal distance to the point of inflexion.

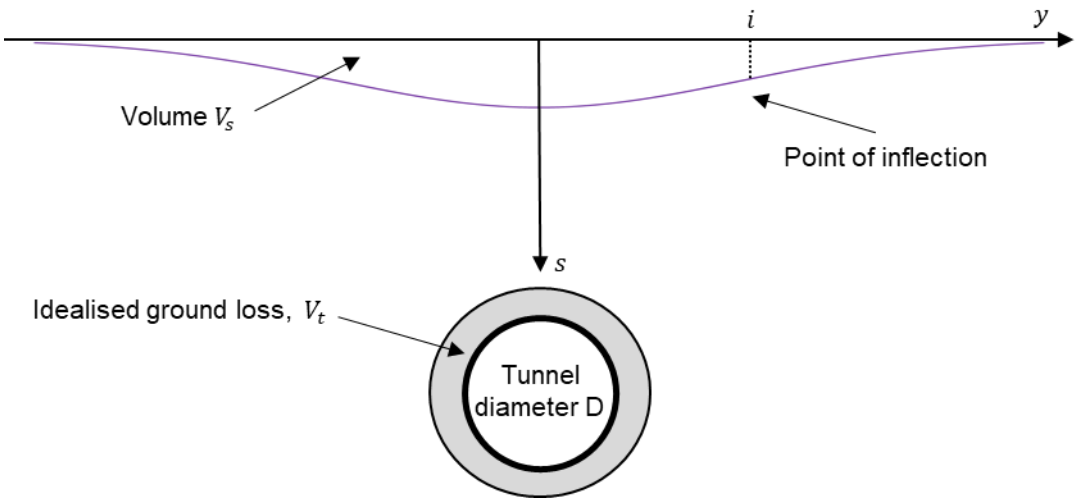

Figure 2. Ground surface settlement trough (Not to scale).

The ground loss, V_t, is the amount of ground lost in the region close to the tunnel (Franza et al., 2019; Mair and Taylor, 1997). When tunnelling in clayey soils, ground movements normally undergo undrained conditions (constant volume) hence $V_s = V_t$. For tunnelling in coarse grain soils, ground deformations are usually under drained conditions, that can result in dilation of the soil, therefore it is highly likely that $V_s < V_t$. Regardless of soil type, Mair & Taylor (1997) suggested that it is convenient to express the volume loss, V_L , in term of the ratio of the volume of the settlement trough, V_S, with the volume of the excavation area, V_{exc}

$$V_S = V_L \times V_{exc}; \quad (3)$$

$$V_{exc} = \pi \frac{D^2}{4}; \quad (4)$$

$$i = Kz_0 \quad (5)$$

where D is the excavation diameter;

K is the dimensionless settlement trough width parameter;

z_0 is the depth from the ground surface to tunnel axis level.

Combining the Equations 2, 3, 4, 5 gives;

$$s = 0.313\frac{V_L D^2}{Kz_0}\exp\left(\frac{-y^2}{2(Kz_0)^2}\right) \quad (6)$$

At a specific location, the diameter, D, and depth, z_0, of the tunnel, the distance from the tunnel centre-line, y, are known leaving the values of the settlement trough width parameter, K, and the volume loss, V_L, to be selected for estimation of the ground surface settlement due to tunnelling. The parameter K depends mainly on the type of soil (O'Reilly & New, 1982). This value can range from 0.2 to 0.7 and influences the width of the overall settlement trough (Mair, 2008; Mair & Taylor, 1997). The volume loss dictates the magnitude of tunnelling-induced ground settlement (Vu et al., 2016). The volume loss magnitude normally ranges from 0.2% to 1% (Wongsaroj et al., 2006; Dimmock, 2003; Wan et al., 2017a; Islam & Iskander, 2021) and in some cases it can be larger than 2% (Shirlaw et al., 2003; The British Tunnelling Society and The Institution of Civil Engineers, 2005) but is mainly dependent on the ground conditions and tunnelling techniques. The latter factor regarding Earth Pressure Balance Machine (EPBM) tunnelling technology is described in the next section followed by an explanation of the resulting volume loss induced during the tunnel construction stages.

EPBM TUNNELLING

The key aspects of an EPBM are depicted in **Figure 3**. The cutterhead excavates the soil in front of the tunnel which then passes into the chamber. Conditioning agents, usually bentonite, foam or polymers, are injected into the plenum (chamber) to mix with the excavated soil to form high viscosity fluid or plasticised spoil (Chapman et al., 2018; Dias & Bezuijen, 2015; Mair, 2008). The resulting plasticised spoil allows easy extraction of the excavated materials. This low water permeability spoil also forms a suitable medium to transfer pressure from the chamber to the tunnel face that allows pressure control in the chamber head (Chapman et al., 2018). An Archimedean screw (screw conveyor) is used to extract the plasticised spoil from the chamber in a controlled manner to maintain stable pressure in the chamber (Chapman et al., 2018). In some cases, conditioning agents are also introduced at the cutterhead and the screw conveyor (Mair, 2008).

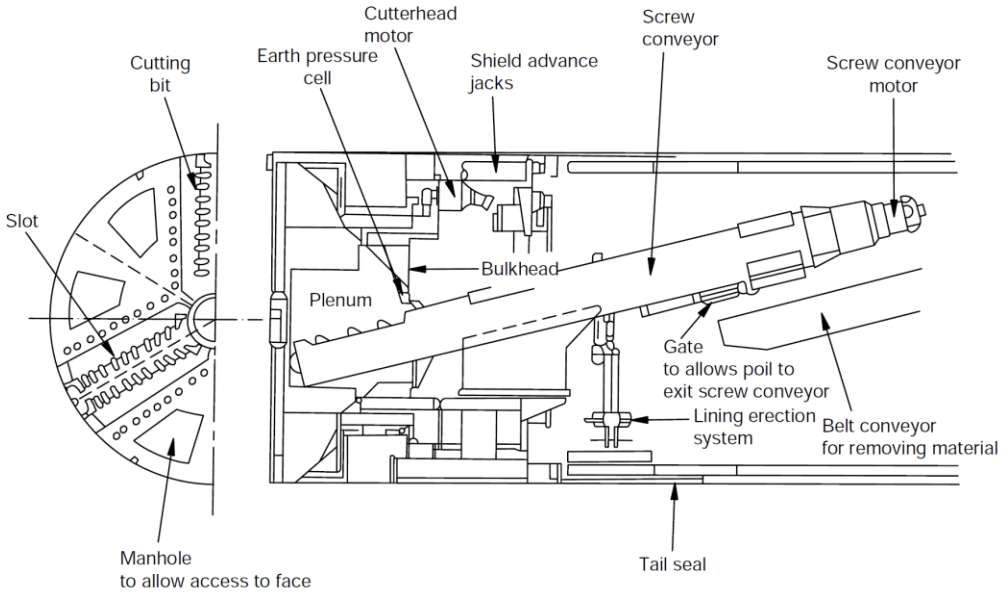

Figure 3. Main components of Earth pressure balance tunnelling machine (Chapman et al., 2018).

The pressure in the chamber can be regulated to provide support, together with the thrust from the machine advancing jacks to the cutterhead, to substantially balance against the soil and pore-water pressures. The screw conveyor plays an important role in controlling the chamber pressure. If the excavation rate is steady, reducing the conveyor speed increases the chamber pressure whereas increasing the conveyor speed reduces the chamber pressure.

The force provided by the jacks is required to overcome the friction on the shield skin together with the force exerted by the pressure in the chamber and drag of the trailing gear (Japan Society of Civil Engineers, 2016; Standing & Selemetas, 2013) in order to thrust the machine forward. When the TBM stops, the force provided by the jacks reduces to a level that is required to balance the pressure exerted by the face.

CHANGES IN PORE-WATER PRESSURE DURING TBM TUNNELLING

The main concern of the project owners and contractors in tunnelling projects are the induced ground movements, buried services and building deformations. However, well reported measurements of the pore-water pressure changes resulting from TBM tunnelling is limited in the literature (Aime et al., 2004; Bezuijen et al., 2017; Broere, 2001; Dias & Bezuijen, 2015; Jin et al., 2022; Kaalberg et al., 2014; Liu et al., 2014; Shi et al., 2021; Wan et al., 2019) .

Figure 4 illustrates typical field pore-water pressure changes, recorded by an in-situ pore pressure transducer (PPT), during tunnel excavation by a slurry TBM in sandy soils (Bezuijen, 2006; Kaalberg et al., 2014). The PPT was pre-installed in the tunnel axis and was destroyed by the TBM upon arriving. Therefore, the measured data is only available until the TBM's face reached the PPT location. The magnitude of the excess pore-water pressure measured by the PPT increases as the TBM approached towards the monitoring section (Aime et al., 2004; Xu & Bezuijen, 2019, 2018). It can be seen that the cyclic loading and unloading when the TBM advances and stops resulted in peak and low values of excessive pore pressure, respectively, i.e. excess pore pressures were measured in front of the TBM during drilling and these decreased to hydrostatic pressure when the drilling stopped.

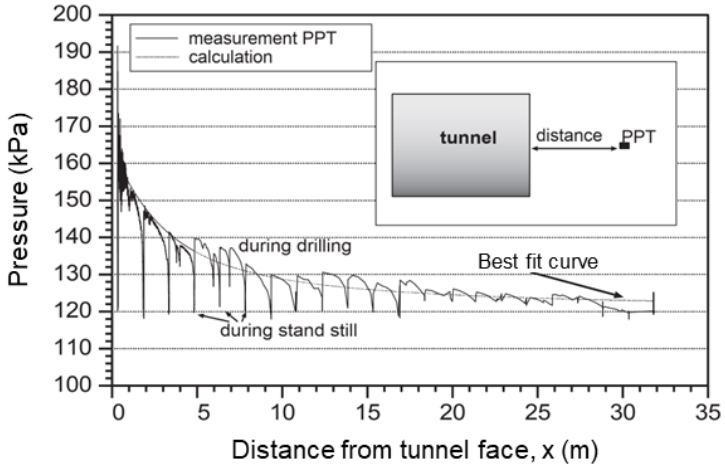

Figure 4. Measured excess pore pressure in front of a TBM in sandy soil (after Bezuijen, 2006).

VOLUME LOSS INDUCED BY TBM TUNNELLING

The tunnel excavation process causes changes to the stress state and pore-water pressure in soils which results in ground movements. Leca et al. (2007) and Wan et al. (2017b) categorise volume loss, induced by TBM tunnelling, into 5 components as depicted in **Figure 5**.

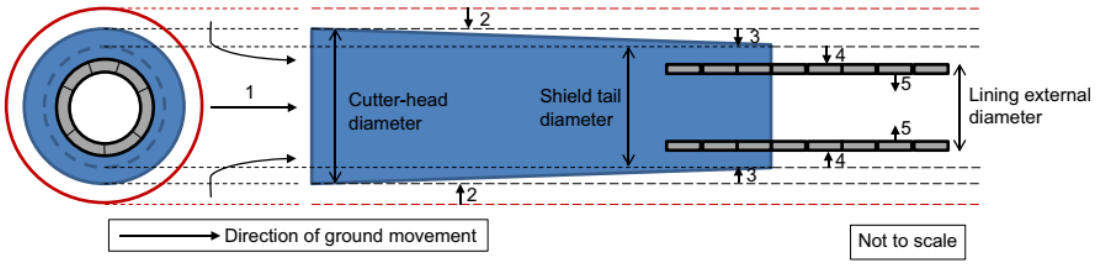

Figure 5. Illustration on components of volume loss (Wan et al., 2017b).

- Component 1 – Face movement: occurs when the support pressure provided by the tunnel face is less than the ground stresses. Therefore, it is critical to maintain substantial pressure at the

tunnel face to minimise the effect of this component. However, using excessive support pressure also results in a higher effective stress in the ground just before the cutting wheel and leads to lower production and higher necessary torque on the cutting wheel. In addition, excessive support pressure may cause 'blow out'. In some cases, contractors were discouraged from using a face pressure larger than 120% of the total overburden pressure (Shirlaw et al., 2003). Long stoppages of TBM with the head empty or partially empty, mainly for maintenance or TBM problems, can cause reduction in face pressure and hence increase in settlement at tunnel face (Biggart & Sternath, 1996; Shirlaw et al., 2003). In addition, unforeseen obstructions in ground, unexpected mixed face soil conditions also contribute to ground movements (Clough and Leca, 1993; Shirlaw, 2016; Tóth et al., 2013; Vergara & Saroglou, 2017) .

- Components 2 and 3 – Movement around the shield body: in order to enable ease of the machine advancing, the diameter of the cutter head is larger than the TBM shield (component 2) and in some cases the shield has the cone shape (component 3) (Biggart & Sternath, 1996; Kavvadas et al., 2017; Liu et al., 2017; Wan et al., 2017b). These two factors result in voids between the excavated soil and the shield skin. Under gravity, soils around the shield have the tendency to settle and close the void. However, it has been reported that the gap between the soil and the TBM shield can be reduced by the tail void grout, that also flows over the smaller diameter part of the shield, resulting in less volume loss (Bezuijen & Bakker, 2009, 2007).
- Component 4 – Tail void closure: as the tunnel linings are erected inside the machine, their diameter is smaller than that for the cutter head and the TBM shield. That in turn creates a void between the final tunnel lining with the excavated soil. In order to minimise the closing up of the void to minimise the consequential settlement, tail void grouting is injected immediately to fill that cavity (Do et al., 2021; Liu et al., 2021). Because of the ground permeation and over-cutting, the actual volume of the injected grout may range from 130–170% of the theoretical tail void volume and sometimes higher in gravel soils (Japan Society of Civil Engineers, 2016). Liu et al. (2017) and Vonk (2020) observed that higher grout volume leads to smaller settlement. Liu et al. (2020) suggested that for shallow tunnels, the ratio should not exceed 145% to avoid penetration of the grout to the ground surface.
- Component 5 – Lining deformation under soils and pore-water stresses, and long-term ground settlement due to consolidation. This component is not considered in this paper.

With strict requirements imposed by the project owners, the common threshold for V_L in practice is normally less than 1% (Wongsaroj et al., 2006) and for congested urban environments the threshold can be less than 0.5%. This paper aims to gain a better insight into prediction of abnormally large settlement by analysing the field data including the geotechnical conditions, geometry and arrangement of the tunnels, the operation parameters of the EPB TBM in the following case study.

THE CASE STUDY

The twin tunnels, in this research, form part of metro line 1 Ben Thanh – Suoi Tien in Ho Chi Minh city, Vietnam (Le et al., 2021). These 781m long twin tunnels were the first tunnels excavated by EPBM in Vietnam. The plan and longitudinal profiles of the tunnels, including the soil conditions along the routes, are depicted in **Figure 6**. The East Bound (EB) tunnel was constructed from 26th May 2017 to 31st October 2017. The EPBM was launched from Bason station (chainage 1586m) and excavated towards the Opera House station (chainage 805m). The TBM was then dismantled and transported back to Bason station for West Bound (WB) tunnel excavation. The WB tunnel was constructed from 26th January 2018 to 29th June 2018 (Le et al., 2020). **Figure 7 a, b** present the advance rate of the TBM in EB and WB tunnels, respectively. At the beginning of the excavation from chainage 1586m, an initial drive of approximately 80m was carried out at a slow rate (**Figure 7**). The EPBM was then stopped at around chainage 1500m for a review of the operational parameters before continuing the main drive for the rest of the route.

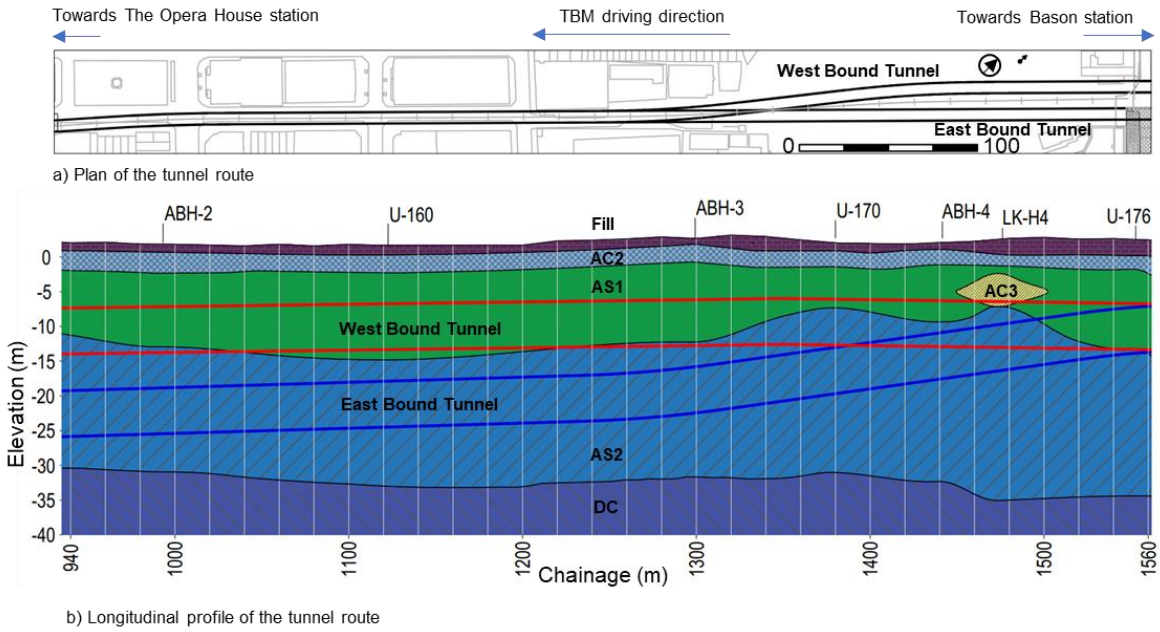

Figure 6. Plan and longitudinal profile of the tunnel route.

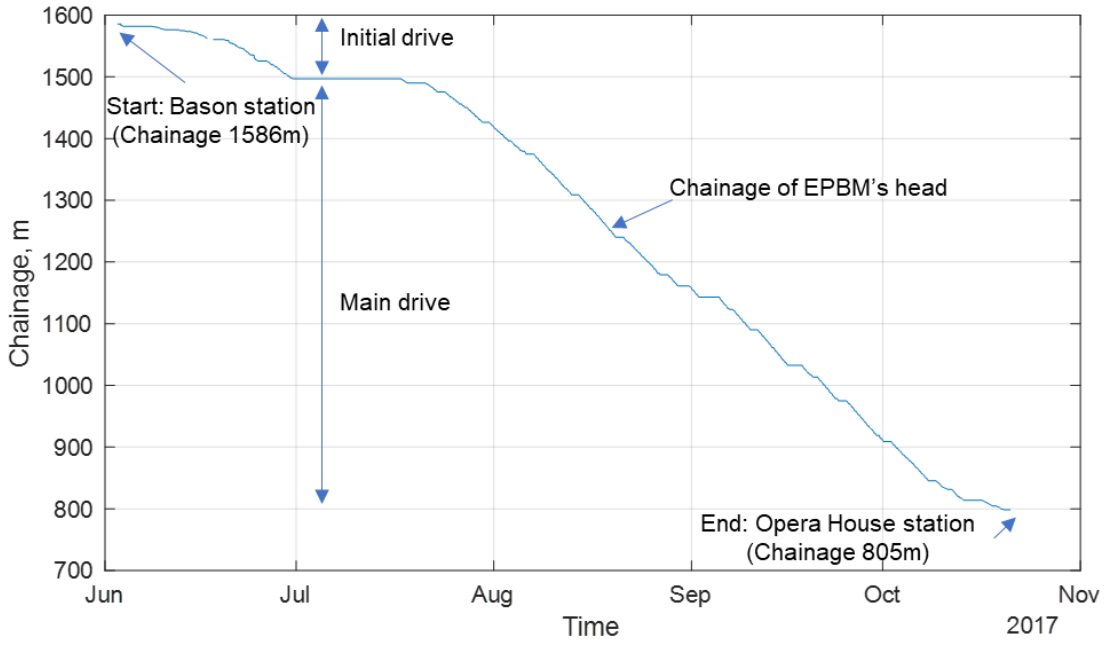

a) TBM advance rate in EB tunnel

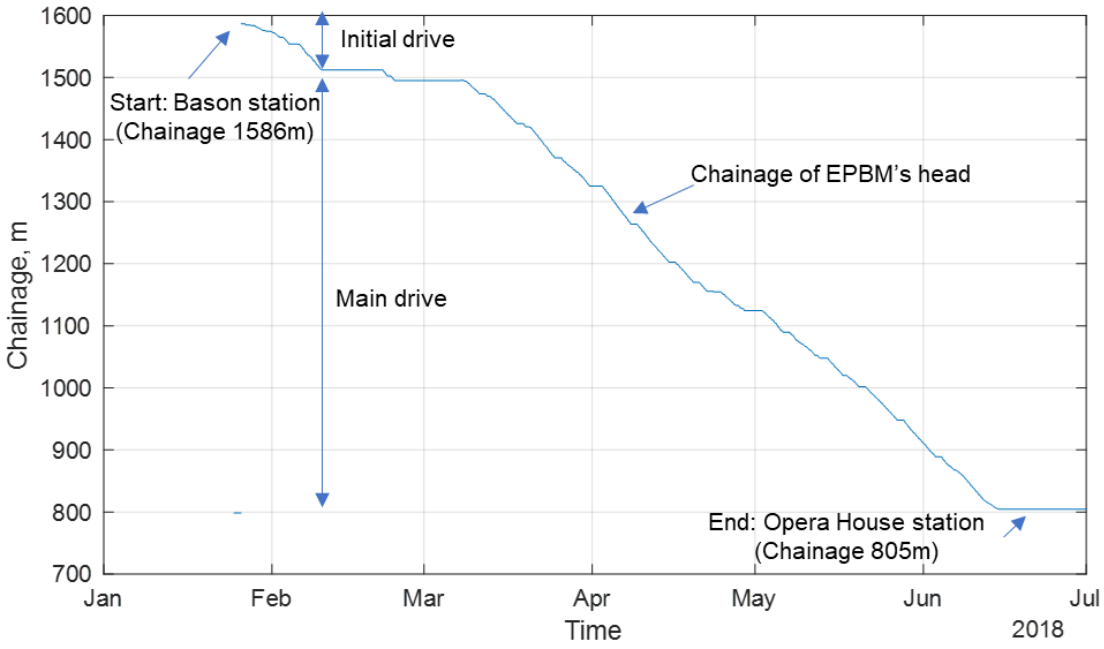

b) TBM advance rate in WB tunnel

Figure 7. TBM advance rate

SITE GEOLOGY

The Soil Investigation report shows that the water table is 2m below the ground surface and the soil consists of five main geological layers (**Figure 6**) as described below:

- Fill: The top soil is mainly fill materials including sand, clay, gravel, brick, concrete. At most of the boreholes, the thickness of this layer is less than 2m. The coefficient of permeability is $k=1x10^{-6}m/s$.

- AC2 (Alluvial clay 2): The soil material is homogenous, very soft fat CLAY, bluish grey. The layer thickness varies from 0 to 4.5m with the average SPT N-value of 2. The coefficient of permeability is $k=1x10^{-9}$m/s.

- AS1 (Alluvial sand): silty fine SAND layer. In general, the soil is very loose to loose, non-homogeneous to homogenous. Silt content ratio decreases with depth and changes to fine sand with silt. The layer thickness varies from 3.2m to 13m with the average SPT N-value of 5. The coefficient of permeability is $k=2x10^{-5}$m/s.

- AS2 (Alluvial sand): This layer is the lowermost in alluvium deposit and above the hard clayey silt of diluvium. The main component of this layer is medium to coarse SAND and the density is from medium dense to dense sand with occasional loose pockets. The thickness varies from 16.9m to 27.8m with the average SPT N-value of 15. The coefficient of permeability is $k=2x10^{-5}$m/s.

- AC3 (Alluvial clay 3): The soil material is homogeneous, firm to stiff fat CLAY with sand. The thickness varies from 0.5m to 7m with the average SPT N-value of 8. The coefficient of permeability is $k=10^{-9}$m/s.

- DC (Diluvium clay): The material consists of homogeneous, hard to very hard, weakly cemented, low permeability, CLAY. The thickness varies from 2.9m to 21.1m with the average SPT N-value of 34. The coefficient of permeability is $k=1x10^{-8}$m/s.

As can be seen from **Figure 6**, most of the EB tunnel is within the sandy soil AS2 while the WB tunnel is within the sandy soil AS1 and at some locations the cross-section of the tunnel encounters mixed soils of AS1 and AS2.

THE TUNNELLING MACHINE

An Earth Pressure Balance Machine (EPBM) was chosen to construct the tunnel as this type of machine is suitable with the sandy ground conditions. The excavation diameter and the shield body diameter are 6.82m and 6.79m, respectively. The length of the EPBM from the cutter face to tail is 8.5m. The tunnel lining rings consist of 6 precast concrete segments including three regular, two counter key and one key segments. Each section of the tunnel lining has a nominal length of 1.2m with the outer and inner diameters of 6.65m and 6.05m, respectively. The machine advances forward by means of 20 hydraulic jacks with a maximum combined thrust of 40,000kN applied to the erected linings to overcome the friction and the face pressure. In addition, along the shield high viscosity bentonite was injected to act as lubricant between the shield extrados and the surrounding soil. At the TBM tail, the void between the tunnel lining extrados and the surrounding soil was filled with a two-part grout consisting of Liquid A and Liquid B. Liquid A was a mix of cement, bentonite, stabilizer and water while Liquid B was a sodium

silicate accelerator. The two-part grout was injected via simultaneous backfill-grouting ports. The grout injection volume was designed to be 130% of the theoretical tail-void volume.

There were four earth pressure gauges installed behind the cutter face to monitor the soil stresses in the vicinity of the tunnel face. The key TBM operation parameters including the face pressure, volumes and pressures of the bentonite at the tunnel face and along the TBM shield, volume and pressure of the tail void grouting, the machine position with time, the hydraulic jack pressures, were recorded at every 5 seconds during the excavation. Those parameters are detailed and analysed together with the field ground surface settlement in the later sections to gain better insight into the tunnelling-induced behaviour of the sandy soils.

THE MONITORING SCHEME

The monitoring points, measured by precise levelling techniques, were arranged approximately perpendicular to the tunnel centre-line (Le et al., 2020). At each section, there were five to eight monitoring points. The ground surface vertical displacement readings were taken once a day when the TBM was within -100m to -10m and twice a day when it was -10m to +40m from the monitoring sections. The negative sign indicates that the TBM was approaching the section whereas the positive sign indicates the TBM was leaving the monitoring section.

FIELD MEASUREMENT ON GROUND SURFACE DISPLACEMENT

Previous research (Le et al., 2016; Le & Taylor, 2018; Nyren, 1998; O'Reilly & New, 1982) indicates that in longitudinal direction along the tunnel centre-line, the ground surface settlement begins to develop and reach a stabilised magnitude when the TBM is within the distance of x from $-z_0$ to $+z_0$, respectively. In this project, the ground surface settlements due to tunnelling are calculated with the baseline when the TBM was at approximately -40m to the monitoring sections which covers the range of the tunnel depth of $z_0 \leq 24m$. The ground surface settlement due to tunnel construction was calculated as the difference between the measured values when the TBM was at -40m and +40m to the monitoring sections.

At some monitoring sections, there were no measurements directly above the tunnel centre-lines where the largest ground vertical displacement normally occurs. Therefore, the method proposed in Jones & Clayton (2013) was used to fit Gaussian approximations to available settlement data, allowing the maximum ground surface vertical displacement, s_{max}, volume loss, V_L, and trough width parameter, K,

211 to be obtained. **Figure 8** presents the Gaussian approximations and corresponding parameters obtained
212 for the EB and WB tunnels at different locations representing geometries where the tunnels were
213 positioned in parallel, diagonal and stacked arrangements.

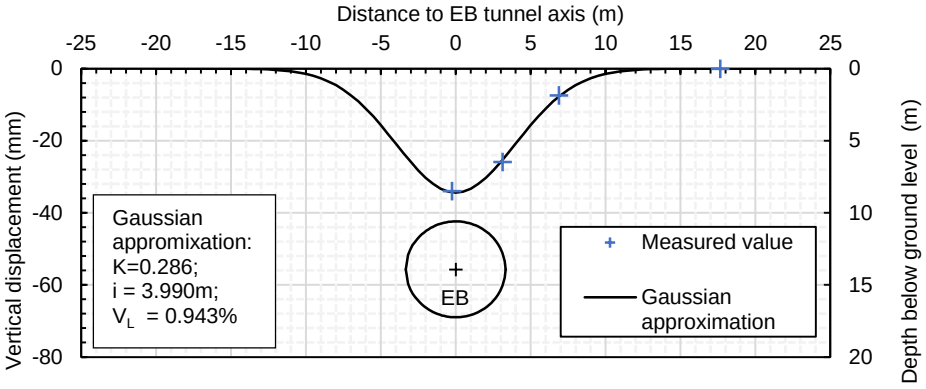

a) Ground surface vertical displacement due to EB tunnel excavation at chainage 1523m

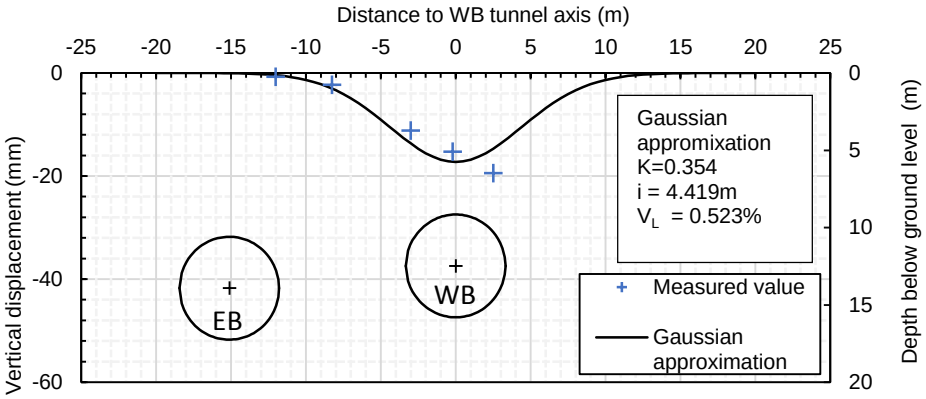

b) Ground surface vertical displacement due to WB tunnel excavation at chainage 1523m

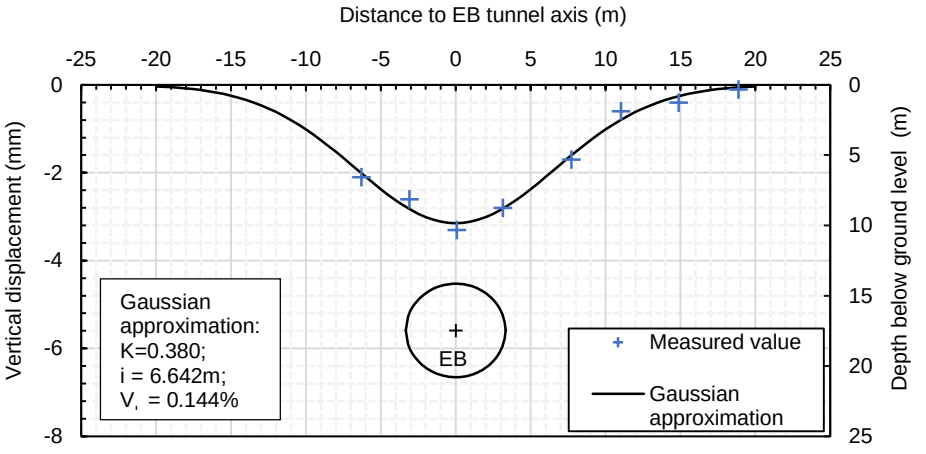

c) Ground surface vertical displacement due to EB tunnel excavation at chainage 1403m

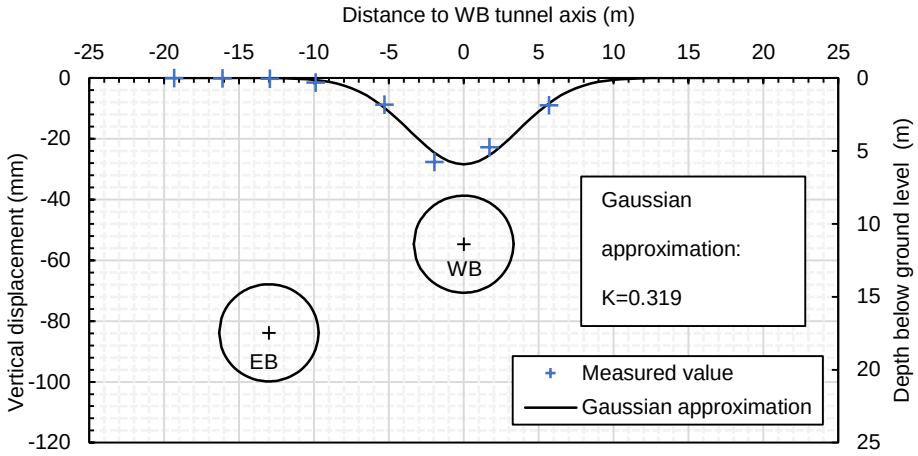

d) Ground surface vertical displacement due to WB tunnel excavation at chainage 1403m

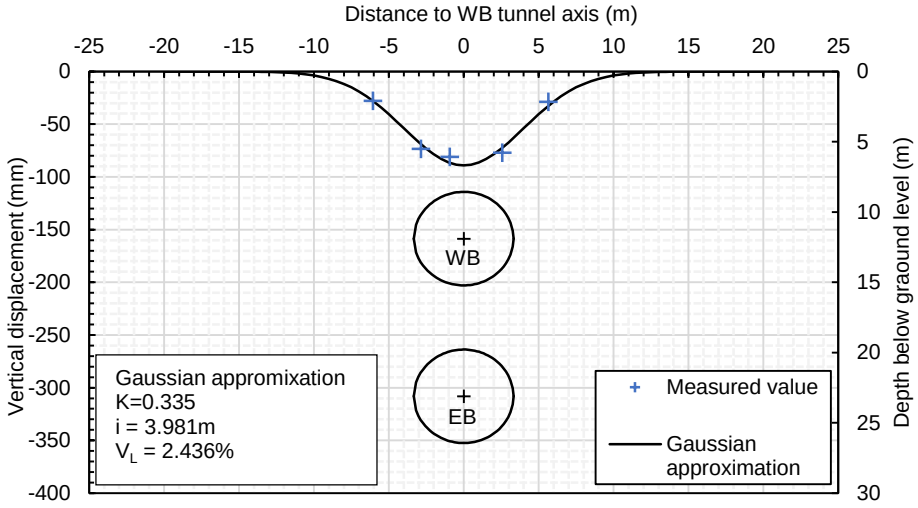

e) Ground surface vertical displacement due to WB tunnel excavation at chainage 1103m

Figure 8. Ground surface settlement troughs and Gaussian approximations.

214

215 The maximum ground surface settlements and the corresponding volume losses along the tunnel route

216 were determined and are presented in **Figure 9 a, b**, respectively.

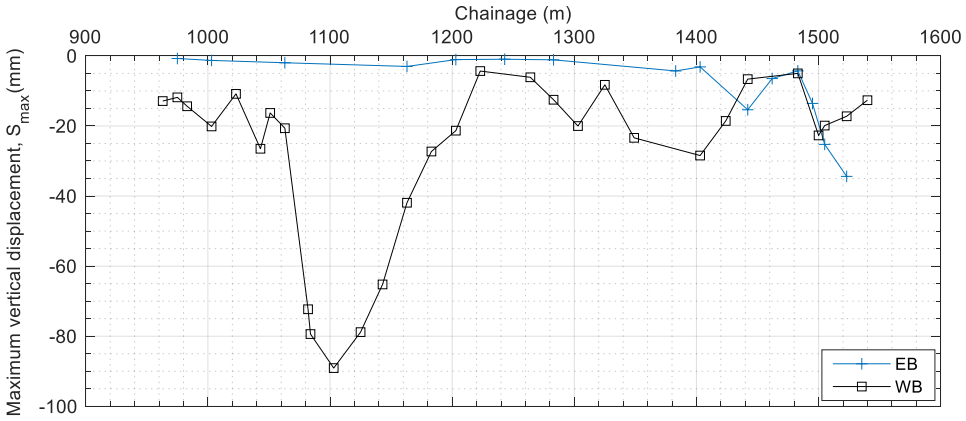

a. Maximum ground surface settlement along the tunnel route

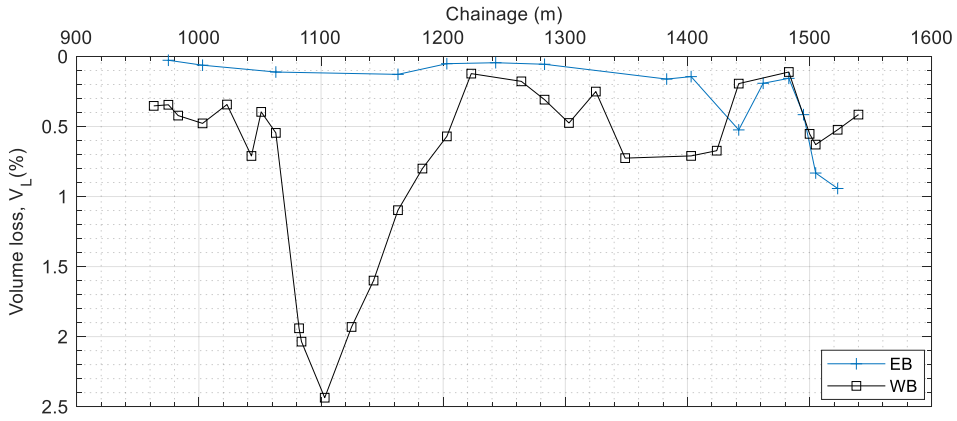

b. Volume loss along the route

Figure 9. Longitudinal ground surface settlement and volume loss.

There were some large ground surface settlements occurring especially from chainage 1080m to 1160m on the WB tunnel with the volume loss up to 2.4%. However, for the EB tunnel, the majority of the surface settlements were less than 5mm and the volume losses were less than 0.2%. There were some exceptions where values of settlements and volume losses were similar to those of the WB tunnel at chainage 1442m and 1520m where the depth of tunnel approached that of the WB tunnel. **Figure 10** depicts typical profiles of $V_{L(x)}$, volume loss when the EPBM was at a distance x to the monitoring section along the tunnel centre-line during the TBM advancement, normalised against V_L, the total volume loss. Also in this figure, is the approximation of the contribution of the volume loss components which are illustrated by the horizontal dashed lines.

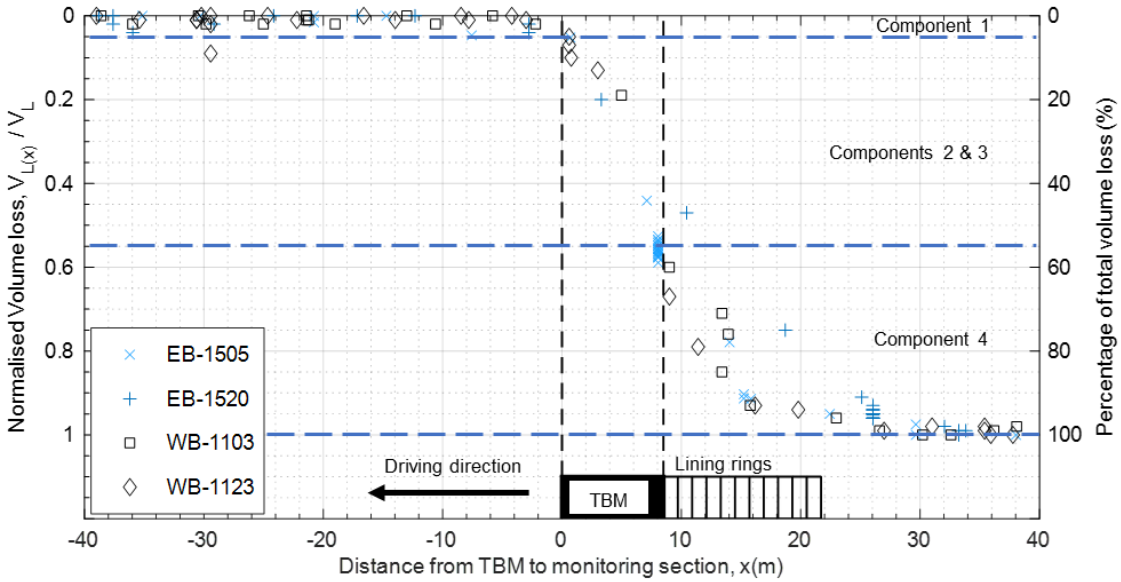

Figure 10. Typical normalised volume losses along the tunnel centre-line

From **Figure 10**, it can be seen that the relative contribution of volume loss components (as defined above and in **Figure 5**), in terms of percentage of the total volume loss, in the EB and WB are consistent. The component 1 contribution is negligible which only accounts for less than 5% of the total volume loss and no further investigation on this component is carried out. On the contrary, more than 95% of the total volume loss were from the components 2, 3 and 4 which are attributed to the volume of void between the excavated soil with the machine shield and the tunnel lining. One of the important factors that governs the magnitude of the components 2 and 3 during volume loss is the stand-up capabilities of the soil before the lining is installed and tail-void grouting is injected. It can be argued that for sandy soil, the stand-up capabilities mostly depend on the density and the degree of saturation of the soil. For saturated sands below the water table (as in this case study) the stand-up capability can be very limited. For component 4, the tail void grouting injection during the excavation to fill the void is of paramount important to reduce the collapse of the soil (Liu, C et al., 2020; Liu, X et al., 2019; Zheng et al., 2021).

Figure 11 presents the measured volume of tail void grouting per ring in the EB and WB tunnels. The theoretical void volume between the excavation perimeter with the tunnel lining extrados, V-void, the design grout volume (130%V-void), and the upper bound of volume 170%V-void (Japan Society of Civil Engineers, 2016; Liu et al., 2019; Vonk, 2020) are depicted as the horizontal dotted line, the solid line and the dashed line, respectively.

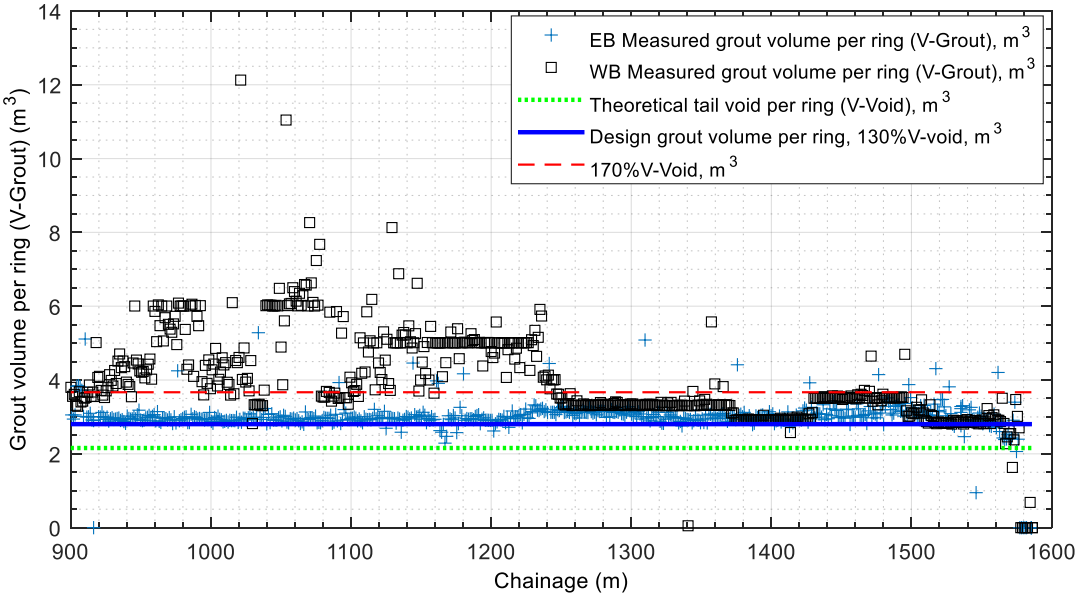

Figure 11. The measured volume of tail void grouting during the tunnel construction.

DISCUSSION

For the EB tunnel route, where most of the TBM excavated through the medium dense to dense sandy soil, AS2, the majority of tail void grout volume was approximate the design grout volume 130%V-void and less than 170%V-void. This is in line with the observations reported by previous research (Japan Society of Civil Engineers, 2016; Liu et al., 2017; Vonk, 2020) and resulted in small volume losses for most of monitoring sections on the EB tunnel route.

However, for WB tunnel route which excavated through the very loose to loose sandy soil, AS1, the tail void grout volume exceeded the values of 170%V-void from chainage 920m to 1240m, and sometimes, reached values up to nearly 6 times the theoretical tail void V-void. Interestingly, despite the larger injected volume of tail void grout (**Figure 11**), the volume losses at those locations were significantly larger than that at other locations in the WB tunnel route and EB tunnel route (**Figure 9b**). There are two possible reasons for this observation considered below.

The first reason was the very loose to loose, fully saturated, sandy soils AS1, might have been weakened by the prior EB tunnel excavation, allowed greater infiltration of tail void grout. This might have reduced the support effectiveness of the grout within the annulus between the lining extrados and the excavated ground for which it was designed.

The second reason was that the cyclic loading from the hydraulic jacks thrusting the TBM forward during the excavation could have caused the cyclic changes in pore-water pressure, reducing the effective stress resulting in weakening and liquefaction of the soil. This, in turn, resulted in significantly larger

settlements and volume losses. As no measurements on pore-water pressure were carried out during the TBM driving, it is not possible to confirm whether liquefactions or soil loosening occurred. However, the pore-water pressure during the TBM driving can be estimated using the measured TBM face pressure, σ_F. When the TBM machine advances forward by the hydraulic jacks the excess pressure in the mixing chamber $\Delta\sigma_F$ is transferred to the pore-water pressure in front of the tunnel face. In the following analysis, it is assumed that $\Delta\sigma_F$ is initially supported by pore-water pressure before transferring to the surrounding soil skeleton (Knappett & Craig, 2019) during standstill and when the distance from the considered location to the TBM increases. As the soil is fully saturated, the excess pore pressure generated in front of the tunnel face, Δu, will be approximately equal to the change in the change in total stress, i.e. change in tunnel face pressure $\Delta\sigma_F$. This assumption may lead to an overestimation of Δu, which is deemed reasonable for a conservative approach to assess liquefaction potential. **Figure 12 a, b** present the measured maximum and minimum hydraulic pressures in a single jack during the EB and WB tunnels for each lining ring. The corresponding measured tunnel face pressures are shown in **Figure 12 c, d**.

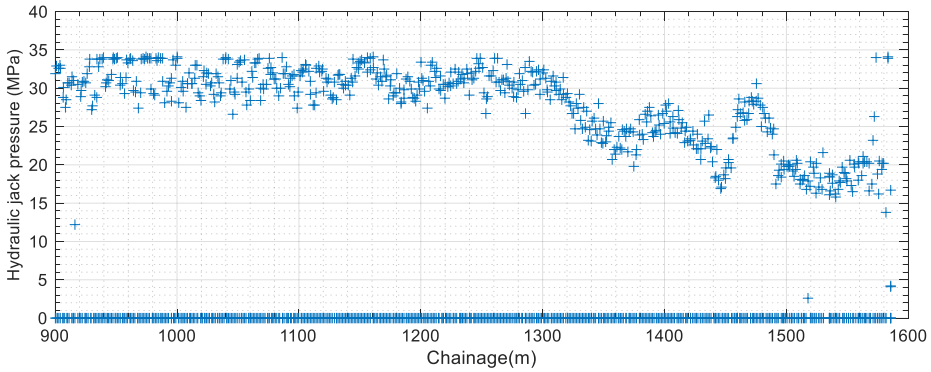

a. Measured hydraulic pressure in a jack during each ring in EB tunnel.

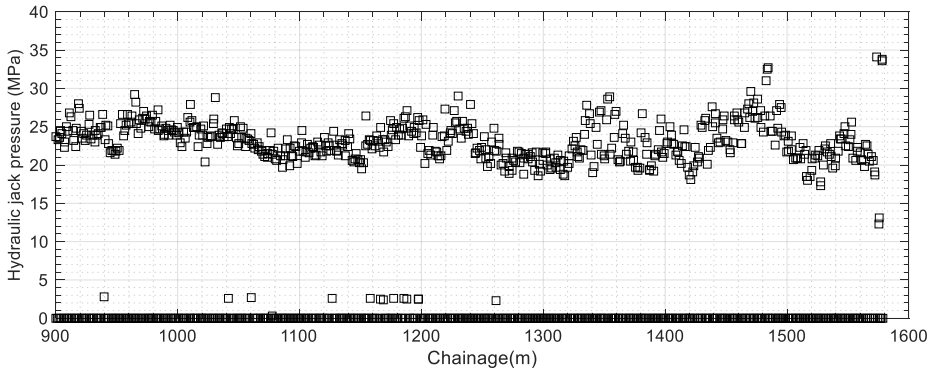

b. Measured hydraulic pressure in a jack during each ring in WB tunnel.

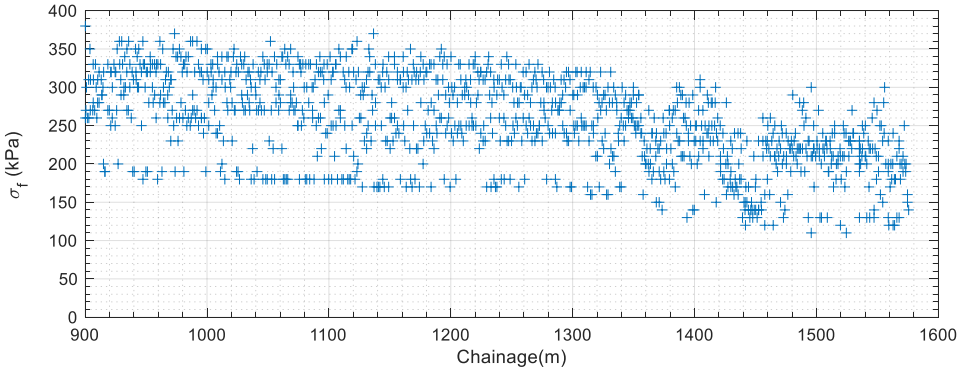

c. Measured tunnel face pressure σ_f during each ring in EB tunnel.

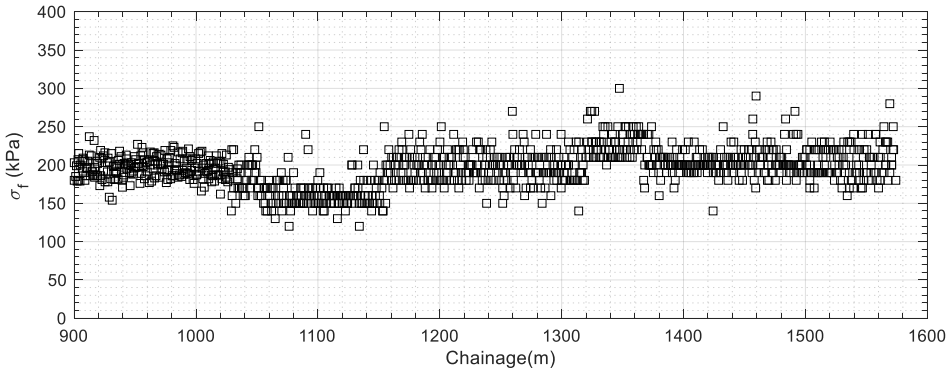

d. Measured tunnel face pressure σ_f during each ring in WB tunnel.

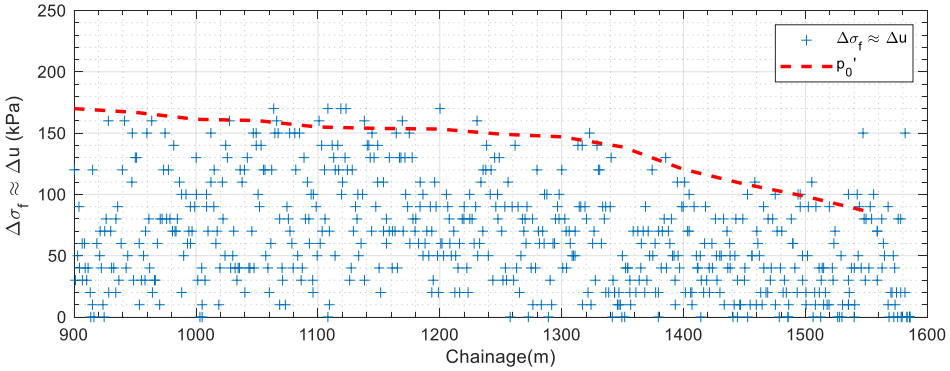

e. Changes in face pressure during each ring in EB tunnel.

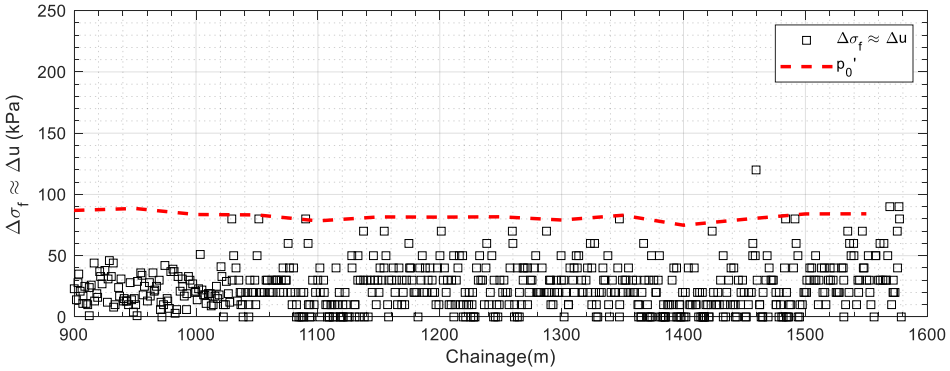

f. Changes in face pressure during each ring in WB tunnel.

Figure 12. The TBM operational variables.

280

The maximum hydraulic pressures occur when all jacks thrust against the previously completed ring to advance the machine forwards. Then, during stoppage for the ring building, the jacks were sequentially retracted, by reducing their hydraulic pressure to zero, to allow for lining segment insertion. It is worth noting that other jacks remained pressurised to support the tunnel face and after the segment installation, the hydraulic pressure in the retracted jacks were increased again to allow for the retraction of other jacks for the new segment installation. Similar observations were reported by (Bezuijen et al., 2017; Yu et al., 2020).

The maximum hydraulic jack pressures for most of the rings in the EB tunnel were up to 34MPa which were larger than that of 30MPa for the WB tunnel (**Figure 12 a, b**). Due to the greater depth of the EB tunnel, hence greater friction and larger face pressure, a larger thrust was required. The effects of the hydraulic jack pressure were also reflected in **Figure 12 c, d, e** and **f** where the measured tunnel face pressures, σ_F, and the amplitude of the changes of the tunnel face pressure, $\Delta\sigma_F$, or the estimated excess pore pressure, Δu, in the EB tunnel was considerably larger than that for the WB tunnel. **Figure 12 e, f** also present the initial mean effective stress p_0' at the tunnel axis level z_0.

$$p_0' = \frac{\sigma_{v0}' + 2\sigma_{h0}'}{3} \tag{7}$$

$$\sigma_{h0}' = \sigma_{v0}' K_0 \tag{8}$$

where σ_{v0}' is the initial vertical effective stress at the tunnel axis level z_0;

σ_{h0}' is the initial horizontal effective stress at the tunnel axis level z_0;

K_0 is the earth pressure coefficient at rest (values of 0.503 to 0.552 were derived from the angle of friction obtained from laboratory tests).

It is worth noting that for both tunnels, some of the estimated Δu values approached the initial mean effective stress p'_0 (**Figure 12 e, f**) which is one of the indicators for liquefaction beside the liquefaction potential index, PL. The next section discusses in more detail the fundamentals of liquefaction in a critical state soil mechanics framework and analyses the relationship between the excess pore-water pressure Δu, liquefaction potential index, PL, with the tunnelling-induced volume loss, V_L.

THE EFFECTS OF LIQUEFACTION

Liquefaction can be caused by either flow or triggered by either monotonic or cyclic loading in undrained condition (Castro & Poulos, 1977; Hanzawa et al., 1979; Ishihara, 1993; Kramer, 1996; Poulos, 1981).

There are common conditions that facilitate the liquefaction reported in the literature. These conditions are coarse grained soil, loose state, high water table, high initial shear stress state, uniform grain size, large amount of round shape particles, small amount of fine particles. In soil mechanics, regardless of the total stress path, depending on the stress history and initial stress state of the soil, in undrained loading the typical effective stress path (**Figure 13**) follows one of three paths from the initial void ratio: (i) dense sand exhibits non flow hardening strain and approaches the steady state line (SSL) at large mean effective stress, p', (Path A1-F, Figure **13**) (ii) medium dense sand undergoes limited liquefaction behaviour by softening first then hardening (Path A2-E, Figure **13**), (iii) loose and very loose sand shows the softening response to the state of very low effective mean stress, p', near the origin of the q-p' plane (Path A3-B-C for monotonic load or path A3-D-C for cyclic loading, **Figure 13**). The equation for deviatoric stress q is presented below;

$$q = \sigma_v' - \sigma_h' \tag{9}$$

In the case of cyclic loading, the cyclic load brings the soil to the unstable state (flow liquefaction surface, FLS) then the effective stresses p'& q drop instantly as under static monotonic loading (Path A3-D-C**,** **Figure 13**). Therefore, the FLS is a reliable predictor for onset of flow liquefaction (Najma & Latifi, 2017).

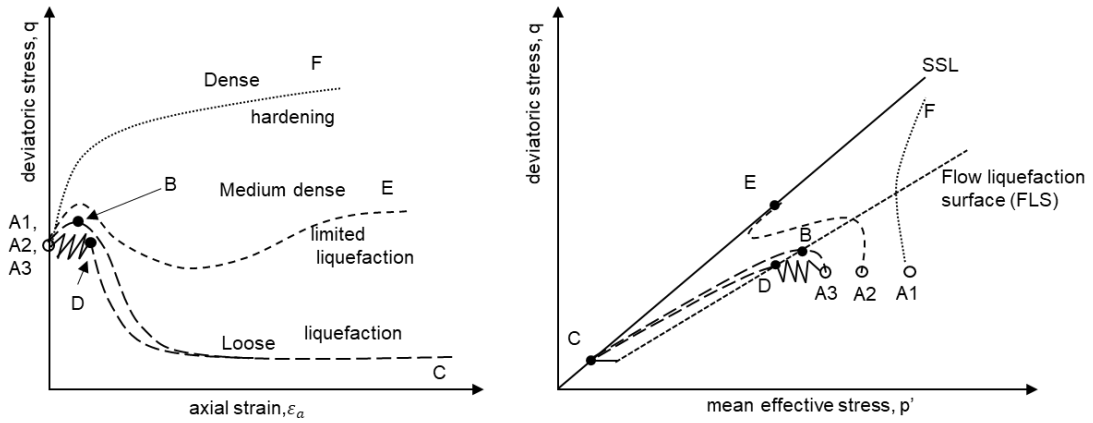

Figure 13. Dilation of dense sand, limited flow liquefaction of medium sand under monotonic loading and flow liquefaction of loose sand initiated by both monotonic and cyclic loading (After Kramer, 1996).

Cyclic liquefaction can occur in a wide range of soil types and states of initial stress. In this case, contractive strain of the soil skeleton is accumulated after each loading-unloading cycle, accompanied by the pore-water pressure build-up, until large deformation is reached. Consequently, the effective stress path moves backward to the origin of the p'-q plane. At this unstable state of very low mean

effective pressure, a small disturbance can easily cause liquefaction (Ishihara et al., 1975; Seed & Lee, 1966; Vaid & Chern, 1983).

In this case study, the water table is approximately 2m below the ground surface. The soil profile along the tunnel route includes the two low permeability clay layers AC2 and DC at the top and bottom respectively. Therefore, for a conservative approach regarding liquefaction possibility, the two fully saturated sandy soil layers in between can be considered as undrained when subjected to the cyclic load from the tunnel driving. This is further confirmed by a long leakage length of 750m to 1000m estimated by the approach suggested by Bezuijen (2017) and Bezuijen et al. (2017).

There have been several qualitative and quantitative methods to assess the liquefaction potential for soils. One of the methods is to conduct advanced cyclic triaxial undrained tests to obtain required parameters to establish the FLS (Najma & Latifi, 2017) as in **Figure 13**. Having the FLS allows the soil at any stress state (p', q), as such subjected to EPBM tunnelling, to be analysed for liquefaction potential. However, such advanced cyclic triaxial tests were not conducted for the project reported in this case study. There are, however, assessment methods for liquefaction potential that use commonly available information such as the soil type, the geology profile and the SPT value, N (Matsuoka et al., 1993; Tokimatsu & Yoshimi, 1983). The use of SPT for evaluation of liquefaction of soil was recommended by previous research and professional bodies (Matsuoka et al., 1993; Railway Technical Research Institute, 2012; New Zealand Geotechnical Society and Ministry for Business Innovation and Employment, 2021; Tokimatsu & Yoshimi, 1983; Youd et al., 2001). The procedure suggested by Iwasaki et al. (1984, 1981) was adopted to estimate liquefaction potential index, PL. This was done by integration of factor of safety to liquefaction, FL, along the depth from the ground surface to the realistic tunnel axis level, z_0, instead of the conventionally accepted 20m depth as proposed by Iwasaki et al. (1984, 1981) and Tatsuoka et al. (1980) to take into account the position of tunnel that affects the ground surface settlement. An example of the detailed calculation of PL is presented in the Appendix. **Figure 14** presents the relationship between the calculated PL with the corresponding volume losses at 14 locations which were within 20m from the nearest borehole.

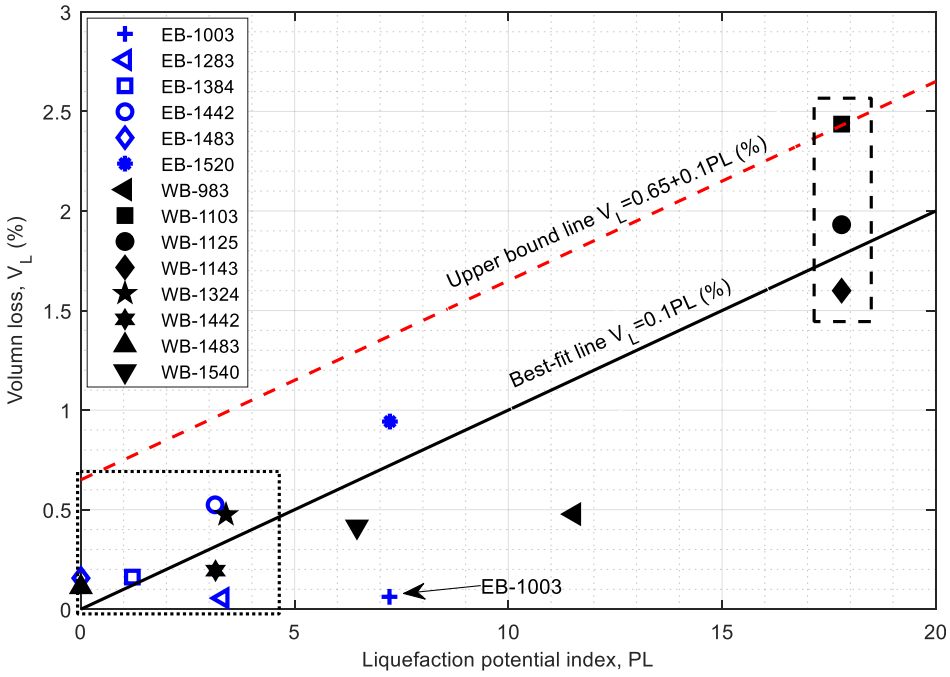

Figure 14. Relationship between the Liquefaction potential index, $\boldsymbol{PL}$, and volume loss, $\boldsymbol{V_L}$.

From **Figure 14**, it can be seen that the volume loss V_L and the liquefaction potential index PL are linearly proportional which can be described by the following equation;

$$V_L = 0.1PL(\%);\ \text{with the mean square error } R^2 = 0.78 \quad (10)$$

Also in **Figure 14**, an upper bound line is suggested for prediction of volume loss from liquefaction potential index PL;

$$V_L = 0.1PL + 0.65(\%); \quad (11)$$

For the largest volume losses ($V_L > 1.5\%$) at WB-1103, WB-1125 and WB-1143 (marked by the dashed box in **Figure 14**), these locations have the same characteristics including very high liquefaction potential index (PL > 15) and the estimated excess pore-water pressures, Δu, were close to or larger than the mean effective stress p_0' (**Figure 12 f**) indicating that the stress path could have reached the flow liquefaction surface and the soil resistance dropped (Najma & Latifi, 2017). These two conditions imply a high possibility of liquefaction which might have loosened the sandy soil around the tunnel lining. That in turn led to excessive backfill grout permeation hence the reduction of the support effectiveness of the grout to the soils around the tunnel lining extrados. This explanation is corroborated by the high volume losses occurred along the tunnel shield and linings (components 2, 3 & 4 in **Figure 10**) and the abnormally large volume of tail void grouting at these locations (**Figure 11**).

For the sections with low Liquefaction potential index (PL < 4, marked by the dotted box in **Figure 14**) the volume losses were generally less than 0.65% and are in line with the commonly observed volume loss induced by TBM tunnelling and no further analysis is carried out. The anomalous data point EB-1003 (annotated in **Figure 14**) is due to the EB tunnel lying in the dense sand AS2 meaning the cyclic loading from TBM excavation attenuates through the dense sand layer and only caused negligible impact to the sensitive loose sand layer AS1. The observation in the normal amount of volume of tail void grouting in **Figure 11** supports this explanation.

CONCLUSION

EBPM tunnelling in saturated sandy soils inherently induces cyclic loads with associated changes in pore-water pressure that may lead to liquefaction or soil loosening. This in turn, potentially, results in large ground surface settlements. Therefore, through assessment of geotechnical data at local boreholes, the use of a liquefaction potential index is recommended. In this research, despite the broad variety of tunnel depths, thickness of soil layers, TBM operational variables, a reasonable relationship between the liquefaction potential index, PL, and volume loss, V_L, (**Figure 14**) along the tunnel route was found. Nevertheless, further research with more data from other projects is recommended to corroborate this finding. **Equations 10** and **11** together with the calculation procedure in Appendix can be useful when estimating where to expect the potential for large settlements caused by EBPM tunnelling in sandy soil. For future tunnelling projects using EPBM in sandy soils, in additions to soil parameters used in the Appendix, it is recommended that cyclic triaxial tests are conducted to gain a better insight into soil behaviour under cyclic loading (Najma & Latifi, 2017). This would allow tunnelling engineers to locate regions with high liquefaction potential index and estimate allowable excess pore-water pressure to avoid liquefaction. Moreover, this would allow necessary soil reinforcement and/or caution to be employed prior to tunnelling. Ground displacement monitoring, pore-water pressure measurements are invaluable in assessing the liquefaction potential and adjusting the TBM operational parameters if needed to ensure safe tunnelling.

ACKNOWLEDGEMENT

This research is funded by Vietnam National Foundation for Science and Technology Development (NAFOSTED) under grant number 107.04-2020.31. This research was also supported by the Global Challenges Research Funding provided by Research England.

REFERENCES

Aime, R., Aristaghes, P., Autuori, P., Minec, S., 2004. 15m diameter tunneling under Netherlands polders, in: ITA World Tunnel Congress 2004-Underground Space for Sustainable Urban Development.

Bezuijen, A., 2017. The influence of the leakage length on the initiation of backward erosion piping, in: Proc. of the 25th Meeting of the European Working Group on Internal Erosion. Delft, the Netherlands. pp. 88–96.

Bezuijen, A., 2006. Influence of pore pressure at tunnel face. Tunnelling. A Decade of Progress. GeoDelft 1995-2005 277–284.

Bezuijen, A., Bakker, K.J., 2009. The influence of flow around a TBM machine, in: Geotechnical Aspects of Underground Construction in Soft Ground. CRC Press, pp. 255–259.

Bezuijen, A., Bakker, K.J., 2007. Bentonite and grout flow around a TBM, in: ITA World Tunnel Congress. pp. 383–388.

Bezuijen, A., Xu, T., Dias, T.G.S., 2017. Pore pressures in front of a slurry shield: development and decline. EURO:TUN 2017 - 4th International Conference on Computational Methods in Tunneling and Subsurface Engineering.

Biggart, A.R., Sternath, R., 1996. Storebaelt Eastern railway tunnel: construction, in: Proceedings of the Institution of Civil Engineers-Civil Engineering. Thomas Telford-ICE Virtual Library, pp. 20–39.

Broere, W., 2001. Tunnel Face Stability & New CPT Applications (PhD Thesis). Delft University of Technology.

Castro, G., Poulos, S.J., 1977. Factors affecting liquefaction and cyclic mobility. Journal of the Geotechnical Engineering Division 103, 501–516.

Chapman, D., Metje, N., Stärk, A., 2018. Introduction to tunnel construction: Second edition, Introduction to Tunnel Construction: Second Edition. CRC Press. https://doi.org/10.1201/9781315120164

Clough, G.W., Leca, E., 1993. EPB shield tunneling in mixed face conditions. Journal of geotechnical engineering 119, 1640–1656.

Dias, T.G.S., Bezuijen, A., 2015. TBM Pressure Models - Observations, Theory and Practice. 15th Pan-American Conference on Soil Mechanics and Geotechnical Engineering - Geotechnical Synergy in Buenos Aires 2015 - Invited Lectures 347–374. https://doi.org/10.3233/978-1-61499-599-9-347

438 Dimmock, P.S., 2003. Tunnelling-induced ground and building movement on the Jubilee Line
439 Extension (PhD thesis). University of Cambridge.
440 Do, N.A., Dias, D., Vu, T.T., Dang, V.K., 2021. Impact of the shield machine's performance
441 parameters on the tunnel lining behaviour and settlements. Environ Earth Sci 80, 1–13.
442 https://doi.org/10.1007/S12665-021-09820-2
443 Franza, A., Marshall, A.M., Zhou, B., 2019. Greenfield tunnelling in sands: The effects of soil density
444 and relative depth. Geotechnique 69, 297–307. https://doi.org/10.1680/JGEOT.17.P.091
445 Hanzawa, H., Itoh, Y., Suzuki, K., 1979. Shear characteristics of a quick sand in the Arabian Gulf.
446 Soils and Foundations 19, 1–15.
447 Ishihara, K., 1993. Liquefaction and flow failure during earthquakes. Geotechnique 43, 351–451.
448 Ishihara, K., Tatsuoka, F., Yasuda, S., 1975. Undrained deformation and liquefaction of sand under
449 cyclic stresses. Soils and foundations 15, 29–44.
450 Islam, M.S., Iskander, M., 2021. Twin tunnelling induced ground settlements: A review. Tunnelling and
451 Underground Space Technology 110, 103614. https://doi.org/10.1016/J.TUST.2020.103614
452 Iwasaki, T., Arakawa, T., Tokida, K.I., 1984. Simplified procedures for assessing soil liquefaction
453 during earthquakes. International Journal of Soil Dynamics and Earthquake Engineering 3, 49–
454 58. https://doi.org/10.1016/0261-7277(84)90027-5
455 Iwasaki, T., Tokida, K., Tatsuoka, F., 1981. Soil liquefaction potential evaluation with use of the
456 simplified procedure, in: International Conference on Recent Advances in Geotechnical
457 Earthquake Engineering and Soil Dynamics, St. Louis. pp. 209–214.
458 Japan Society of Civil Engineers, 2016. Standard specifications for tunneling: Shield tunnel. Japan
459 Society of Civil Engineers Tokyo.
460 Jin, Dr.H., Yuan, Dr.D., Jin, Dr.D., Wu, Mr.J., Wang, Dr.X., Han, Dr.B., Mao, Dr.J., 2022. Shield
461 kinematics and its influence on ground settlement in ultra-soft soil: a case study in Suzhou.
462 https://doi.org/10.1139/cgj-2021-0603. https://doi.org/10.1139/CGJ-2021-0603
463 Jones, B.D., Clayton, C., 2013. Guidelines for Gaussian curve-fitting to settlement data. Underground.
464 The Way to the Future 645–652. https://doi.org/10.1201/b14769-90
465 Kaalberg, F.J., Ruigrok, J.A.T., de Nijs, R., 2014. TBM face stability & excess pore pressures in close
466 proximity of piled bridge foundations controlled with 3D FEM. Geotechnical Aspects of
467 Underground Construction in Soft Ground 555–560.

Kavvadas, M., Litsas, D., Vazaios, I., Fortsakis, P., 2017. Development of a 3D finite element model for shield EPB tunnelling. Tunnelling and Underground Space Technology 65, 22–34. https://doi.org/10.1016/J.TUST.2017.02.001

Knappett, J., Craig, R.F., 2019. Craig's Soil Mechanics. CRC Press. https://doi.org/10.1201/9781351052740

Kramer, S.L., 1996. Geotechnical earthquake engineering. Pearson Education India.

Le, B.T., Kuriki, M., Phan, Q., Taylor, N., 2020. An empirical analysis on measured ground surface settlement induced by TBM tunnelling in Ho Chi Minh city, Lecture Notes in Civil Engineering. https://doi.org/10.1007/978-981-15-2184-3_38

Le, B.T., Nadimi, S., Goodey, R.J., Taylor, R.N., 2016. System to measure three-dimensional movements in physical models. Geotechnique Letters 6. https://doi.org/10.1680/jgele.16.00073

Le, B.T., Nguyen, N.T., Divall, S., Goodey, R.J., Taylor, R.N., 2021. Modified gap method for prediction of TBM tunnelling-induced soil settlement in sand-a case study, in: Geotechnical Aspects of Underground Construction in Soft Ground. CRC Press, pp. 584–589.

Le, B.T., Taylor, R.N., 2018. Response of clay soil to three-dimensional tunnelling simulation in centrifuge models. Soils and Foundations 58. https://doi.org/10.1016/j.sandf.2018.03.008

Leca, E., New, B., Reporter, G., 2007. Settlements induced by tunneling in Soft Ground. Tunnelling and Underground Space Technology 22, 119–149. https://doi.org/10.1016/j.tust.2006.11.001

Liu, C., Cui, J., Zhang, Z., Liu, H., Huang, X., Zhang, C., 2021. The role of TBM asymmetric tail-grouting on surface settlement in coarse-grained soils of urban area: Field tests and FEA modelling. Tunnelling and Underground Space Technology 111. https://doi.org/10.1016/J.TUST.2021.103857

Liu, C., Li, J., Zhang, Z., Li, P., Cui, J., Liu, H., Yang, Y., 2020. Model tests on tail-grouting process during URUP shield tunneling in soft soil. Tunnelling and Underground Space Technology 103, 103451. https://doi.org/10.1016/j.tust.2020.103451

Liu, C., Zhang, Z., Regueiro, R.A., 2014. Pile and pile group response to tunnelling using a large diameter slurry shield-Case study in Shanghai. https://doi.org/10.1016/j.compgeo.2014.03.006

Liu, C., Zhang, Z.X., Kwok, C.Y., Jiang, H.Q., Teng, L., 2017. Ground Responses to Tunneling in Soft Soil Using the URUP Method. Journal of Geotechnical and Geoenvironmental Engineering 143, 04017023. https://doi.org/10.1061/(asce)gt.1943-5606.0001695

Liu, X., Wang, F., Huang, J., Wang, S., Zhang, Z., Nawnit, K., 2019. Grout diffusion in silty fine sand stratum with high groundwater level for tunnel construction. Tunnelling and Underground Space Technology 93, 103051. https://doi.org/10.1016/J.TUST.2019.103051

Mair, R.J., 2008. Tunnelling and geotechnics: New horizons. Geotechnique 58, 695–736. https://doi.org/10.1680/geot.2008.58.9.695

Mair, R.J., Taylor, R.N., 1997. Bored tunnelling in the urban environment, in: Fourteenth International Conference on Soil Mechanics and Foundation Engineering. 14th ICSMGE (Hamburg) Conference 19. Vol 4, pp. 2353–2380.

Matsuoka, M., Midorikawa, S., Wakamatsu, K., 1993. Liquefaction potential mapping for large area using the digital national land information. Journal of Structural and Construction Engineering (Transactions of AIJ) 452, 39–45. https://doi.org/10.3130/AIJSX.452.0_39

Najma, A., Latifi, M., 2017. Predicting flow liquefaction, a constitutive model approach. Acta Geotech 12, 793–808. https://doi.org/10.1007/s11440-016-0517-x

New Zealand Geotechnical Society, Ministry for Business Innovation and Employment, 2021. Earthquake geotechnical engineering practice, Module 3: Identification, assessment and mitigation of liquefaction hazards.

Nyren, R.J., 1998. Field measurements above twin tunnels in London Clay (PhD thesis). Imperial College London.

O'Reilly, M.P., New, B.M., 1982. Settlements above tunnels in the United Kingdom - their magnitude and prediction., in: Tunnelling '82. Papers Presented at the 3rd International Symposium. pp. 173–181.

Peck, R.B., 1969. Deep excavations and tunneling in soft ground. Proc. 7th ICSMFE 225–290.

Poulos, S.J., 1981. The steady state of deformation. Journal of the Geotechnical Engineering Division 107, 553–562.

Railway Technical Research Institute, 2012. Design standards for railway structures and commentary (seismic design) (In Japanese).

Schmidt, B., 1969. Settlements and ground movements associated with tunneling in soil (PhD thesis). University of Illinois.

Seed, H.B., Lee, K.L., 1966. Liquefaction of saturated sands during cyclic loading. Journal of the Soil Mechanics and Foundations Division 92, 105–134.

528 Shi, J., Wang, F., Zhang, D., Huang, H., 2021. Refined 3D modelling of spatial-temporal distribution of
529 excess pore water pressure induced by large diameter slurry shield tunneling. Comput Geotech
530 137, 104312. https://doi.org/10.1016/j.compgeo.2021.104312
531 Shirlaw, J.N., 2016. Pressurised TBM tunnelling in mixed face conditions resulting from tropical
532 weathering of igneous rock. Tunnelling and Underground Space Technology 57, 225–240.
533 https://doi.org/10.1016/J.TUST.2016.01.018
534 Shirlaw, J.N., Ong, J.C.W., Rosser, H.B., Tan, C.G., Osborne, N.H., Heslop, P.E., 2003. Local
535 settlements and sinkholes due to EPB tunnelling. Proceedings of the Institution of Civil Engineers
536 - Geotechnical Engineering 156, 193–211. https://doi.org/10.1680/geng.2003.156.4.193
537 Standing, J.R., Selemetas, D., 2013. Greenfield ground response to EPBM tunnelling in London Clay.
538 Géotechnique 63, 989–1007. https://doi.org/10.1680/geot.12.P.154
539 Sugiyama, T., Hagiwara, T., Nomoto, T., Nomoto, M., Ano, Y., Mair, R.J., Bolton, M.D., Soga, K.,
540 1999. Observations of Ground Movements during Tunnel Construction by Slurry Shield Method
541 at the Docklands Light Railway Lewisham Extention-East London. Soils and Foundations.
542 https://doi.org/10.3208/sandf.39.3_99
543 Tatsuoka, F., Iwasaki, T., Tokida, K. ichi, Yasuda, S., Hirose, M., Imai, T., Kon-no, M., 1980. Standard
544 penetration tests and soil liquefaction potential evaluation. Soils and Foundations 20, 95–111.
545 https://doi.org/10.3208/SANDF1972.20.4_95
546 The British Tunnelling Society and The Institution of Civil Engineers, 2005. Closed-Face Tunnelling
547 Machines and Ground Stability.
548 Tokimatsu, K., Yoshimi, Y., 1983. Empirical Correlation of Soil Liquefaction Based on SPT N-Value
549 and Fines Content. Soils and Foundations 23, 56–74.
550 https://doi.org/10.3208/SANDF1972.23.4_56
551 Tóth, Á., Gong, Q., Zhao, J., 2013. Case studies of TBM tunneling performance in rock-soil interface
552 mixed ground. Tunnelling and Underground Space Technology 38, 140–150.
553 https://doi.org/10.1016/j.tust.2013.06.001
554 Vaid, Y.P., Chern, J.-C., 1983. Effect of static shear on resistance to liquefaction. Soils and
555 foundations 23, 47–60.
556 Vergara, I.M., Saroglou, C., 2017. Prediction of TBM performance in mixed-face ground conditions.
557 Tunnelling and Underground Space Technology 69, 116–124.
558 https://doi.org/10.1016/j.tust.2017.06.015
559 Vonk, M., 2020. Grouting the tail void (Master thesis). Delft University of Technology.

560 Vu, M.N., Broere, W., Bosch, J., 2016. Volume loss in shallow tunnelling. Tunnelling and Underground
561 Space Technology 59, 77–90. https://doi.org/10.1016/J.TUST.2016.06.011
562 Wan, M. S.P., Standing, J.R., Potts, D.M., Burland, J.B., 2017a. Measured short-term ground surface
563 response to EPBM tunnelling in London Clay. Geotechnique 67, 420–445.
564 https://doi.org/10.1680/jgeot.16.P.099
565 Wan, M.S.P, Standing, J.R., Potts, D.M., Burland, J.B., 2017b. Measured short-term subsurface
566 ground displacements from EPBM tunnelling in London Clay. Géotechnique 67, 748–799.
567 https://doi.org/https://doi.org/10.1680/jgeot.SIP17.P.148
568 Wan, M.S.P., Standing, J.R., Potts, D.M., Burland, J.B., 2019. Pore water pressure and total horizontal
569 stress response to EPBM tunnelling in London Clay. Geotechnique 69, 434–457.
570 https://doi.org/10.1680/JGEOT.17.P.309
571 Wongsaroj, J., Borghi, F.X., Soga, K., Mair, R.J., Sugiyama, T., Hagiwara, T., Bowers, K.H., 2006.
572 Effect of TBM driving parameters on ground surface movements: Channel Tunnel Rail Link
573 Contract 220, in: Geotechnical Aspects of Underground Construction in Soft Ground. London:
574 Taylor & Francis Group, pp. 335–341.
575 Xu, T., Bezuijen, A., 2019. Bentonite slurry infiltration into sand: Filter cake formation under various
576 conditions. Geotechnique 69, 1095–1106. https://doi.org/10.1680/jgeot.18.P.094
577 Xu, T., Bezuijen, A., 2018. Analytical methods in predicting excess pore water pressure in front of
578 slurry shield in saturated sandy ground. Tunnelling and Underground Space Technology 73,
579 203–211. https://doi.org/10.1016/j.tust.2017.12.011
580 Youd, T.L., Idriss, I.M., Andrus, R.D., Arango, I., Castro, G., Christian, J.T., Dobry, R., Finn, W.D.L.,
581 Leslie F. Harder, Jr., Hynes, M.E., Ishihara, K., Koester, J.P., Liao, S.S.C., William F. Marcuson,
582 I., Martin, G.R., Mitchell, J.K., Moriwaki, Y., Power, M.S., Robertson, P.K., Seed, R.B., Kenneth
583 H. Stokoe, I., 2001. Liquefaction Resistance of Soils: Summary Report from the 1996 NCEER
584 and 1998 NCEERNSF Workshops on Evaluation of Liquefaction Resistance of Soils. Journal of
585 Geotechnical and Geoenvironmental Engineering 127, 817–833.
586 https://doi.org/10.1061/(ASCE)1090-0241(2001)127:10(817)
587 Yu, H., Mooney, M., Bezuijen, A., 2020. A simplified excavation chamber pressure model for EPBM
588 tunneling. Tunnelling and Underground Space Technology 103, 103457.
589 https://doi.org/10.1016/J.TUST.2020.103457

590 Zheng, D., Bezuijen, A., Thewes, M., 2021. An experimental study on foam infiltration into saturated
591 sand and its consequence for EPB shield tunneling. Tunnelling and Underground Space
592 Technology 111. https://doi.org/10.1016/J.TUST.2021.103878
593

594 **LIST OF FIGURES**

595 Figure 1. Idealisation of tunnelling induced soil displacement (after Le & Taylor, 2018). 3
596 Figure 2. Ground surface settlement trough. 4
597 Figure 3. Main components of Earth pressure balance tunnelling machine (Chapman et al., 2018). 6
598 Figure 4. Measured excess pore pressure in front of a TBM in sandy soil (after Bezuijen, 2006). 7
599 Figure 5. Illustration on components of volume loss (Wan et al., 2017b). 7
600 Figure 6. Plan and longitudinal profile of the tunnel route. 9
601 Figure 7. TBM advance rate 10
602 Figure 8. Ground surface settlement troughs and Gaussian approximations. 14
603 Figure 9. Longitudinal ground surface settlement and volume loss. 15
604 Figure 10. Typical normalised volume losses along the tunnel centre-line 16
605 Figure 11. The measured volume of tail void grouting during the tunnel construction. 17
606 Figure 12. The TBM operational variables. 19
607 Figure 13. Dilation of dense sand, limited flow liquefaction of medium sand under monotonic loading
608 and flow liquefaction of loose sand initiated by both monotonic and cyclic loading (After Kramer, 1996).
609 21
610 Figure 14. Relationship between the Liquefaction potential index, PL, and volume loss, VL. 23
611

APPENDIX – CALCULATION PROCEDURE FOR LIQUEFACTION POTENTIAL INDEX

The liquefaction potential index, PL, can be calculated by weighted integration of the safety rate to liquefaction, F, with depth z as depicted in **Figure A1** and described by the Equation A.1 (Iwasaki et al., 1981, 1984);

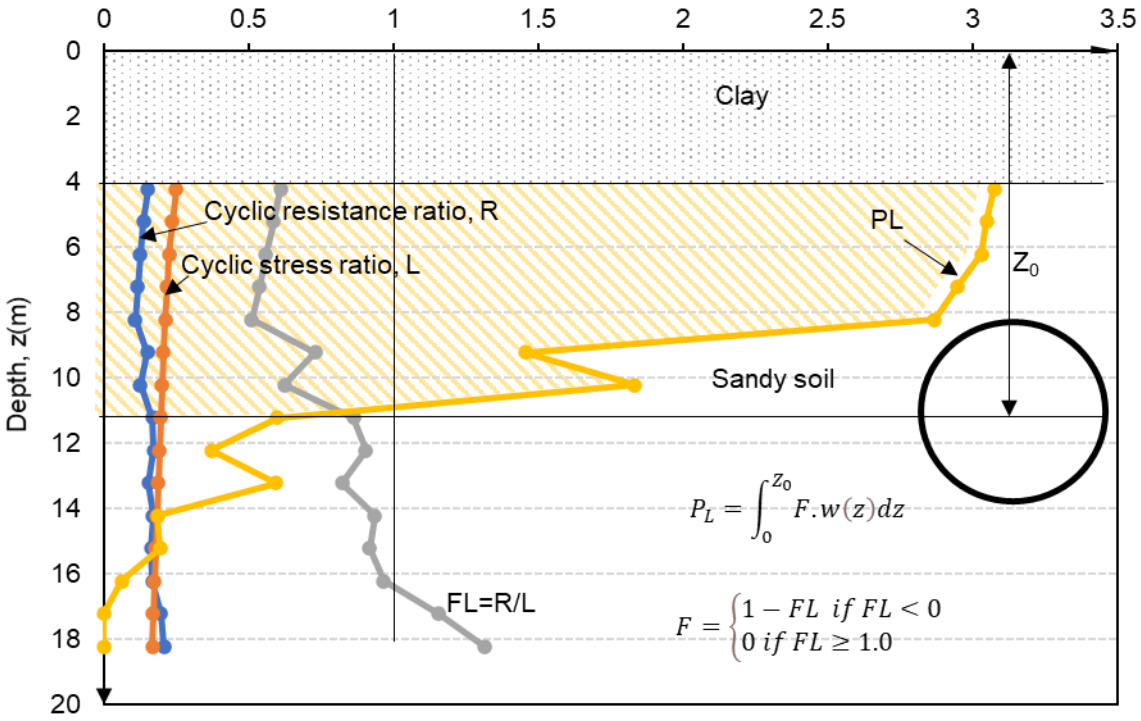

Figure A1. Definition of FL and PL

$$PL = \int_0^{Z_0} F.w(z)dz \tag{A.1}$$

Where $w(z)$: the weight function in accordance with depth z, larger weight is assigned for surficial upper depth;

$$w(z) = 10 - 0.5z \tag{A.2}$$

z: depth from the ground surface (m).

$$F = \begin{cases} 1 - FL \ \ if\ FL < 0 \\ 0\ if\ FL \geq 1.0 \end{cases} \tag{A.3}$$

FL is the factor of liquefaction resistance;

$$FL = \frac{R}{L} \tag{A.4}$$

L is the seismic shear stress ratio;

$$L = \frac{\alpha}{g}.\frac{\sigma_v}{\sigma_v'}.\gamma_d \quad \text{(A.5)}$$

where

α: peak ground acceleration, in the region of Ho Chi Minh city for sandy soil: $\alpha = 0.11448\ g$

σ_v : vertical total stress (kN/m^2)

σ_v' : vertical effective stress (kN/m^2)

γ_d : reduction coefficient, $\gamma_d = 1 - 0.015z$, depth below ground level (m)

For the dynamic shear strength ratio R , there are several methods to determine R using different sets of geotechnical inputs. In this paper, the method suggested by (Iwasaki et al., 1981, 1984) is used and presented as below;

The dynamic shear strength ratio R is calculated with cyclic triaxial strength ratio R_L from following correction formula

$$R = C_w.R_L \quad \text{(A.6)}$$

Cyclic triaxial strength ratio R_L is defined experimentally from the following formula

$$R_L = \begin{cases} 0.0882\sqrt{N_a/1.7} & if\ \ N_a < 14 \\ 0.0882\sqrt{N_a/1.7} + 1.6 \times 10^{-6}(N_a - 14)^{4.5} & if\ 14 \le N_a \end{cases} \quad \text{(A.7)}$$

N_a : amended N-value taken into account the effect of grain size

For sandy soil, then N_a is calculated as:

$$N_a = C_1 N_1 + C_2 \quad \text{(A.8)}$$

In which $C_1 \& C_2$ are the coefficients considering the fine content F_c of the soil

$$C_1 = \begin{cases} 1.0 & if\ 0\% \le F_c \le 10\% \\ \dfrac{F_c + 40}{50} & if\ \ 10\% \le F_c < 60\% \\ \dfrac{F_c}{20} - 1 & if\ 60\% \le F_c \end{cases} \quad \text{(A.9)}$$

$$C_2 = \begin{cases} 1.0 & if\ 0\% \le F_c < 10\% \\ F_c - 10 & if\ 10\% \le F_c \end{cases} \quad \text{(A.10)}$$

For gravelly soil:

$$N_a = \left[1 - 0.36 \log_{10}\left(\frac{D_{50}}{2}\right)\right] N_1 \quad \text{(A.11)}$$

With D_{50} : mean grain diameter (mm)

Normalised N-value (N_1) for effective upper load pressure of 1kgf/cm^2 =100 kPa is given below.

$$N_1 = 1.7 \frac{N}{\sigma'_v/100 + 0.7} \quad \text{(A.12)}$$

N: raw SPT count at site

The coefficient C_w is defined according to the type of the seismic motion as follows.

a) Type 1: Seismic motion by great inter-plate earthquake with low occurrence frequency

Large amplitude acts for a long time repeatedly $C_w = 1.0$.

b) Type 2: Seismic motion by large inland earthquake with very low occurrence frequency

$$C_w = \begin{cases} 1.0 \ \ (R_L \leq 0.1) \\ 3.3R_L + 0.67 \ \ (0.1 < R_L \leq 0.4) \\ 2.0 \ \ (0.4 < R_L) \end{cases} \quad \text{(A.13)}$$

In this case study, the area is subjected to Type 2 hence C_w is estimated by equation A.13.

The PL results obtained from Iwasaki's method for boreholes a long WB tunnel is presented in Table A1. The locations of the boreholes can be referred to **Figure 6** in the manuscript.

Table A1. PL results along the WB tunnel route.

Borehole	Chainage	PL
ABH-2	1000	11.5
U-160	1120	17.8
ABH-3	1300	3.4
U-170	1380	0.0
ABH-4	1440	3.2
LKH-4	1480	0.0
U-176	1540	6.5

In the manuscript, **Figure 14** uses the PL values from Table A1 for the monitoring sections that are within approximately 20m from the borehole.

For practical application, PL can be used as an indicator for the liquefaction potential as below;

$PL = 0$: Liquefaction potential is very low;

$0 < PL \leq 5$: Liquefaction faction potential is low;

$5 < PL \leq 15$: Liquefaction faction potential is high, caution should be taken during tunnel excavation process;

$15 > PL$: Liquefaction faction potential is very high, caution should be taken during tunnel excavation process.